INTERNATIONAL JOURNAL OF HYDROGEN ENERGY 35 (2010) 11216–11228

Available at www.sciencedirect.com

ScienceDirect

journal homepage: www.elsevier.com/locate/he

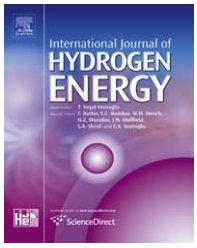

Development of Fe–Ni/YSZ–GDC electrocatalysts for application as SOFC anodes: XRD and TPR characterization and evaluation in the ethanol steam reforming reaction

Raigenis da Paz Fiuza, Marcos Aurélio da Silva, Jaime Soares Boaventura*

Energy and Materials Science Group – GECIM, Institute of Chemistry, Physical Chemistry Department, Universidade Federal da Bahia, 41170290 Salvador, Bahia, Brazil

ARTICLE INFO

Article history:
Received 12 December 2009
Received in revised form
28 June 2010
Accepted 3 July 2010
Available online 5 August 2010

Keywords:
Anode
Carbon deposition
Ethanol
Solid oxide fuel cell (SOFC)
Iron–nickel catalyst
Reforming

ABSTRACT

Electrocatalysts based on Fe–Ni alloys were prepared by means of modified Pechini and physical mixture methods and using on a composite of Yttria Stabilized Zirconia (YSZ) and Gadolinia-Doped Ceria (GDC) as support. The former method was based on the formation a polymeric precursor that was subsequently calcined; the later method was based on the mixture of NiO and the support. The resulting composites had 35 wt.% metal load and 65 wt.% support (70 wt.% YSZ and 30 wt.% GDC mixture) (cermets). The samples were then characterized by Temperature-Programmed Reduction (TPR) and X-Ray Diffraction (XRD) and evaluated in the ethanol steam reforming at 650 °C for 6 h in the temperature range of 300–900 °C. The XRD results showed that the bimetallic sample calcined at 800 °C formed a mixed oxide ($NiFe_2O_4$) with a spinel structure, which, after reduction in hydrogen, formed Ni–Fe alloys. The presence of Ni was observed to decrease the final reduction temperature of the $NiFe_2O_4$ species. The addition of iron to the nickel anchored to YSZ–GDC increased the hydrogen production and inhibited carbon deposition. The resulting bimetallic 30Fe5Ni sample reached an ethanol conversion of about 95% and a hydrogen yield up to 48% at 750 °C. In general, ethanol conversion and hydrogen production were independent of the metal content in the electrocatalyst. However, the substitution of nickel for iron significantly reduced carbon deposition on the electrocatalyst: 74, 31, and 9 wt.% in the 35Ni, 20Fe15Ni, and 30Fe5Ni samples, respectively.

1. Introduction

Solid oxide fuel cells (SOFC) are devices that convert the chemical energy of gaseous fuels, such as hydrogen, natural gas and ethanol, to electricity through electrochemical processes. Due to their high efficiency, design modularity and environmentally friendly nature, SOFCs are considered one of the most promising energy converters. In addition, SOFCs, when compared to other fuel cell systems, offer the possibility of internal reforming of ethanol or hydrocarbon fuels, which may occur directly on the anode. This phenomenon gives SOFC greater flexibility in terms of fuel choice, which is one of its main advantages [1–5].

One of the challenges of using fuel cells as a commercial alternative for electricity generation is the fact that they usually require high purity hydrogen as fuel. Hydrogen is predominantly produced by steam reforming reactions of natural gas or higher hydrocarbons, which contain approximately 100 ppm carbon monoxide, requiring additional purification to satisfy fuel cell demands. Therefore, high purity hydrogen production

* *Corresponding author.*
E-mail addresses: raigenis@ufba.br (R. da Paz Fiuza), bventura@ufba.br (J.S. Boaventura).
0360-3199/$ – see front matter
doi:10.1016/j.ijhydene.2010.07.026

and distribution add additional levels of complexity to the overall system. However, oxidation of ethanol and hydrocarbons directly on SOFC anodes has been experimentally demonstrated by a number of authors [6–10]. It is well-known that Ni–YSZ cermet anodes of SOFC have excellent catalytic properties and stability to H_2 oxidation under SOFC operation conditions [11,12]. However, as Ni is also a good catalyst for hydrocarbon cracking reactions, the use of ethanol or hydrocarbon fuels in a SOFC with a Ni-based anode results in carbon deposition with rapid, irreversible cell degradation [13–16]. As a result, Ni–YSZ cermet anodes can only be used for ethanol or hydrocarbon fuel if a high excess of steam to fuel is present in the cell anode in order to ensure complete fuel reforming and to suppress carbon deposition. Therefore, the development of an anode material for SOFCs that operates on ethanol or hydrocarbons at lower carbon to water ratios (at least close to the stoichiometric ratio) is widely recognized to be an important technical objective [3,7,8,17,18].

Park and Virkar [19] recently studied the use of composites of iron and nickel supported on GDC ($Gd_{0.1}Ce_{0.9}O_{2-\delta}$) for SOFC anodes. These cells were prepared with Gd_2O_3-doped ceria as the electrolyte and a mixture of Sr-doped $LaCoO_3$ (LSC) and GDC as the cathode functional layer. This system showed maximum power densities as high as 0.68 W cm^{-2}, measured at 650 °C with the cell fueled with hydrogen. Huang et al. [3] studied a Fe–Ni/ScSZ (Scandia Stabilized Zirconia) composite as an anode material for SOFC running on ethanol fuel, showing that carbon formation was greatly suppressed on SOFC anodes based on Fe–Ni alloys compared to Ni-based anodes. These authors then evaluated a unitary SOFC prepared with an anode made with the Fe–Ni/ScSZ composite, a ScSZ compound as electrolyte and $(Pr_{0.7}Ca_{0.3})_{0.9}MnO_3$ as the cathode. The constructed cell had a power density of 430 mW cm^{-2} at 850 °C when fed with ethanol vapor. Therefore, a composite made of Ni and Fe appears to offer a good compromise between satisfactory catalytic activity and carbon deposition formation.

Many authors have developed methods for the preparation of composites, each of which creates SOFC anodes with different properties [20,21]. Martins et al. [20] found that the physical mixture and the modified Pechini methods promoted stronger interactions between NiO and YSZ. Although the impregnation method led to a larger NiO coating on the YSZ surface, the NiO species obtained from this method were more easily reducible, regardless of the calcination temperature used. This property can be considered a great advantage, as the reduction of NiO particles happens *in situ* at the beginning of cell operation and easier reduction should help the SOFC reaction start faster. They also observed that the NiO and YSZ particle sizes influenced the composite reduction behavior more than the synthesis method.

Ribeiro et al. [21] studied a Ni/YSZ cermet material with 30 wt.% of NiO prepared using two different methods, co-precipitation and combustion, followed by calcination at 600, 800 or 1000 °C. The authors observed that the mean crystallite size of NiO was smaller for the combustion samples (20–33 nm), showing that this method yielded samples with higher Ni dispersion. The combustion samples also presented a more homogeneous particle size distribution, mainly at high calcination temperatures. Incidentally, these studies demonstrated that the evaluation of the composites in their powder form helped to understand and improve the development of SOFC anodes, especially those fed with hydrocarbon or alcohol.

As previously noted, the main challenges for the technical and commercial viability of SOFCs are the development of materials that allowed the cell to operate at temperatures around 700 °C and anode with special properties. These novel anodes should be able to reform carbon containing fuels directly on their surface, oxidize hydrogen at high rates and, mostly important, minimize, or completely suppressed, carbon formation, in addition to their electronic and ionic conductivity. The search of the SOFC anode with all this properties has been the subject of many works [2,3]. Furthermore, ethanol has particular appeals as a source of electrical energy, because it is a renewable fuel and has a much lower environmental impact than the fossil fuels [5].

This work presents the development of a cermet, with catalytic properties, based on nickel, as the reforming and oxidation catalyst, and iron as the conducting metal phase, because of its lower activity for carbon formation [2]. The ceramic material was based on a mixture of YSZ and GDC, which presents good ionic conductivity around 700 °C, as well as good sinterability [2]. The catalysts were prepared by Pechini method, known to give small crystallite particles [22] that would further inhibited carbon formation. The catalysts were tested in the ethanol steam reforming reaction, since the SOFC power might be related to the catalyst performance for hydrogen production [23]. Surprisingly, the developed catalysts gave better performance and lower carbon formation that could be expected from its nickel load. Further electrochemical properties of the cermet, as ionic and electronic conductivity at SOFC conditions fuel with ethanol, should be analyzed, however the developed electrocatalyst gather several characteristics that makes it a material with very high potential to be a SOFC anode.

2. Experimental

2.1. Sample preparation

Ni–Fe/YSZ–GDC cermet powders with 35 wt.% metal supported on 65 wt.% YSZ–GDC (70 wt.% YSZ and 30 wt.% GDC) were prepared using two methods detailed described in the following paragraphs: modified Pechini and physical mixture methods and using a composite of Yttria Stabilized Zirconia (YSZ) and Gadolinia-Doped Ceria (GDC) as support (Table 1). The former method was based on the formation of a polymeric precursor that was subsequently calcined; the later method was based on the mixture of NiO and the support. The samples were then characterized by Temperature-Programmed Reduction (TPR) and X-Ray Diffraction (XRD) and evaluated in the ethanol steam reforming at 650 °C for 6 h as well as at a variable temperature in the range of 300–900 °C.

YSZ [$(Y_2O_3)_{0.08}(ZrO_2)_{0.92}$], with a surface area of 6–9 $m^2\ g^{-1}$ and a particle size of 0.5–0.7 μm, and GDC ($Ce_{0.9}Gd_{0.1}O_2$), with a surface area of 5–8 $m^2\ g^{-1}$ and a particle size of 0.3–0.5 μm powders, were obtained from Fuel Cell Material®.

Table 1 – Sample descriptions and nominal metal contents. The percentage of available nickel and iron were based on the metallic content. The YSZ–GDC mixture was 65 wt.% for all samples studied.

Preparation method	Metal loading		Sample name
	%Ni	%Fe	
Pechini	0	35	35Fe
	5	30	30Fe5Ni
	15	20	20Fe15Ni
	35	0	35Ni
Physical	35	0	35NiC

2.1.1. *Modified Pechini method for sample preparation*

An aqueous solution of nickel [$Ni(NO_3)_2.6H_2O$] and iron nitrates [$Fe(NO_3)_3.9H_2O$] (both from Merck®) was added to a solution of citric acid (CA, Merck®). The resulting solution was stirred, heated to 60 °C, and the powdered support (YSZ-GDC) was slowly added. Ethylene glycol (EG, Merck®) was added to the resulting solution in a molar ratio of CA/EG = 1/4 and a molar ratio of CA/metallic ion = 6/1, followed by stirring at 60 °C for 1 h. The temperature was then raised to 90 °C and kept at this temperature until the final volume was reduced to half of the initial value, and a polymeric gel was formed.

The polymeric gel was calcined at 350 °C ± 0.25% at a heating rate of 1 °Cmin^{-1} from 25 to 350 °C. Afterwards, the obtained brown solid was ground in a ball mill for 24 h and finally calcined at 900 °C for 3 h with a heating rate of 5 °C min^{-1} from 25 to 900 °C ± 0.25%.

2.1.2. *Physical method for sample preparation*

YSZ–GDC was mixed with NiO in the presence of a small amount of ethanol and the mixture was stirred for 24 h in a ball mill. The powder formed was calcined at 900 °C ± 0.25% for 3 h with a heating rate of 5 °Cmin^{-1} from 25 to 900 °C.

2.2. *Sample characterization*

Crystallographic characterization of the samples was performed by X-ray diffraction (XRD) in a Shimadzu XRD 6000 with Cu Kα radiation (40 kV and 40 mA) between 10 and 80° ± 0.01° at a rate of 0.25°min^{-1}. Sample crystallite sizes were then determined from the Scherrer equation [24].

Temperature-programmed reduction (TPR) analysis was performed on a system consisting of a U-shaped quartz reactor, an oven with temperature control and a gas analysis system with a thermal conductivity detector (TCD). A sample of about 30 mg was placed in the quartz reactor and heated from ambient temperature to about 1000 °C ± 0.25% at a heating rate of 10 °Cmin^{-1} under a flow of 1.5% H_2/argon at a rate of 30 ml min^{-1} ± 1% To this apparatus was attached a trap for removing the water formed in the TPR reaction, and the certified hydrogen mixture used in the reaction was obtained from Linde. The TPR system was calibrated by measuring the supplied and consumed hydrogen flow, enabling the quantitative determination of the reduction extension of the oxides. The obtained spectra were processed with deconvolution techniques to determine the different species present in the solids.

The measurements of specific surface area were performed in a Micromeritics ASAP 2020 using 0.2 g of each sample preheated to 300 °C for 1 h under a nitrogen flow. The typical error associated with measures of specific surface area by this technique was between 5 and 10%.

2.3. *Catalytic tests*

The samples were evaluated in the steam reforming of ethanol at reaction temperatures between 300 and 900 °C ± 0.25% and also as a function of time on the stream at 650 °C ± 0.25% for 6 h in a quartz micro-reactor. In these experiments, the mass of carbon formed during the reaction was measured and the carbon formation was calculated as the difference between the mass of the catalyst after the reforming reaction and the initial mass of the reduced catalyst. Initially, 200 mg ± 0.1% of catalyst was reduced *in situ* with hydrogen (10 mol%) diluted in nitrogen from 30 to 800 °C ± 0.25% with a heating rate of 10 °Cmin^{-1}. The final temperature was then maintained for 30 min. All ethanol steam reforming runs were conducted with nitrogen as the carrier gas at a flow rate of 60 mL min^{-1} ± 1% using a mass flow controller. A previously prepared aqueous ethanol solution, with a molar ratio of water to ethanol equal to 3:1, was injected into the reaction system through a syringe-type pump. The injection rate for this solution was 2 mL h^{-1} ± 0.35%, which corresponded to 1.78 × 10^{-2} mol of ethanol per hour. The gaseous products of the reaction were analyzed by gas chromatography using a Carboxen® 1010 column and a thermal conductivity detector (TCD) in series with a flame ionization detector (FID) [23]. The gas chromatograph (SHIMADZU GC-17A) had a system for automatic sample injection that was programmed to collect and inject a sample every 10 min. During analysis, both injector and detector were maintained at 150 °C and the column at 105 °C. The quantification of the chromatographic analysis was made using an external standard, which gave a typical error of 0.7% for ethanol [25].

2.4. *Data analysis*

The ethanol conversion (X_{ET}) in the steam reforming of ethanol was calculated according to the definition of Hill [26] and given by equation (2.1).

$$X_{ET} = \left(V^0 C^0_{ET} - V^S C^S_{ET}\right)/\left(V^0 C^0_{ET}\right) \quad (2.1)$$

where V^0 and V^S are the total gas flow at the inlet and outlet of the reactor, respectively, both measured at normal temperature and pressure, and C^0_{ET} and C^S_{ET} are, respectively, the concentrations of ethanol in the inlet and outlet of the reactor. The later was measured by gas chromatography, and the former was calculated from the amount of ethanol and water injected in the reactor as an aqueous solution.

The inlet volume (V^0) was calculated from the measured carrier gas plus the injected ethanol and water vapors. The outlet volume (V^S) was calculated from the inlet volume, to which was added the volume variation of the reforming reaction, assuming that all the ethanol reacted. Considering the chromatography analyses, the errors associated with the measurement of the total ethanol molar flow of the inlet and

outlet were 1 and 4%, respectively. Therefore, the ethanol conversion was measured with an error of approximately 5%.

The hydrogen yield was also calculated according to the definition of Hill [26] and given by equation (2.2).

$$Y_{H2} = N^{S}_{H2}/\left[6\left(N^{0}_{ET} - N^{0}_{ET}\right)\right] \quad (2.2)$$

where N^{s}_{H2} is the number of moles of hydrogen formed, N^{0}_{ET} is the number of moles of ethanol in the reactor inlet, and N^{E}_{ET} is the number of moles of ethanol that did not react [27]. Following the same reasoning developed to estimate the error in the ethanol conversion measurements, the mass balance for ethanol and hydrogen was typically within ±5% error range. Therefore, the hydrogen yield was also measured with a typical error of 5%.

3. Results and discussion

3.1. Catalyst characterization

Table 2 shows the specific surface areas of the samples. In general, there was no significant variation in the specific surface area after the incorporation of nickel and iron oxide phases. Among the monometallic nickel samples, the surface area varied from 4 $m^2\ g^{-1}$ in the sample prepared by the physical mixing method to 8 $m^2\ g^{-1}$ in the sample prepared by the Pechini method.

Fig. 1 shows the X-ray diffraction of 35Ni and 35NiC samples, as well as the YSZ–GDC support, which was subject to preparation and calcination conditions similar to those of the samples. From the position of diffraction peaks, the different methods of sample preparation caused no significant change in the nature of the crystalline phases present in the support material. In both samples, nickel oxide (NiO) in the cubic form (JCPDS 78-0643) was formed following the calcination step, and YSZ (JCPDS 82-1246) and GDC (JCPDS 75-0161) were both also found to be in the cubic form.

Fig. 2 shows the XRD patterns for the samples containing iron. Interestingly, only hematite (Fe_2O_3), in a rhombohedral structure (JCPDS 87-1166), was present in the 35Fe sample. The XRD patterns of the bimetallic samples, 20Fe15Ni and 30Fe5Ni, indicated the coexistence of hematite, with a rhombohedral structure, and a mixed oxide of nickel and iron ($NiFe_2O_4$) in a spinel-type cubic structure (JCPDS 74-2081). Qualitative observation of the relative intensity of the diffraction peaks for the bimetallic samples suggested that the mixed oxide was the major phase and the hematite was the minor in the

Table 2 – Specific surface areas of the prepared cermet samples.

Samples	Area (m^2/g)
YSZ–GDC	5
35Ni	8
35Ni C	4
35Fe	3
20Fe15Ni	3
30Fe5Ni	4

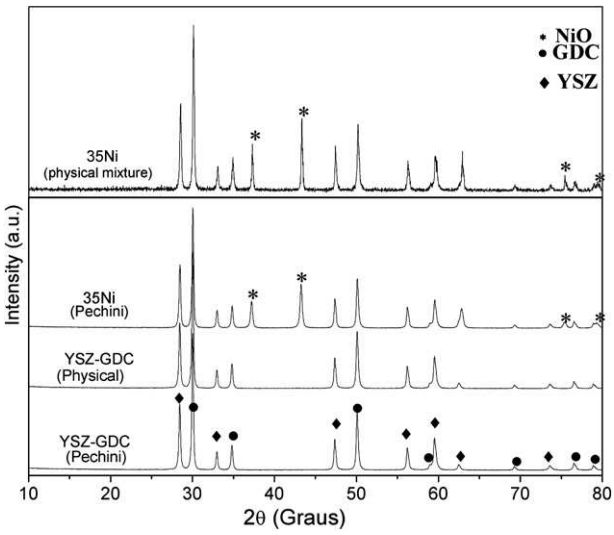

Fig. 1 – XRD patterns of Ni/YSZ–GDC prepared by the physical mixture and Pechini methods and YSZ–GDC composite powders after calcination.

20Fe15Ni sample. However, this relationship was reversed for the 30Fe5Ni sample. These observed qualitative relationships were consistent with the nominal sample compositions. Fig. 2 also indicated that there were no reflections in the XRD patterns, suggesting the occurrence of secondary phases.

Fig. 3 shows the XRD patterns of the samples after being subjected to reduction in the presence of hydrogen at 800 °C. In the 35Ni sample, nickel was crystallized as a face centered cubic (FCC) structure (JCPDS 87-0712) and metallic iron in the 35Fe sample was crystallized in a body-centered cubic (BCC) structure (JCPDS 87-0722).

The XRD diffractogram for the 20Fe15Ni sample (Fig. 3), along with the disappearance of peaks associated with pure nickel and iron, presented three new peaks at positions

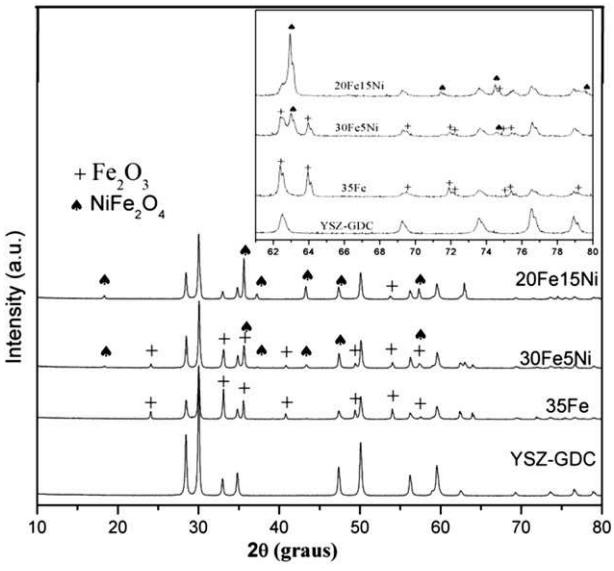

Fig. 2 – XRD patterns of composite powders after calcination.

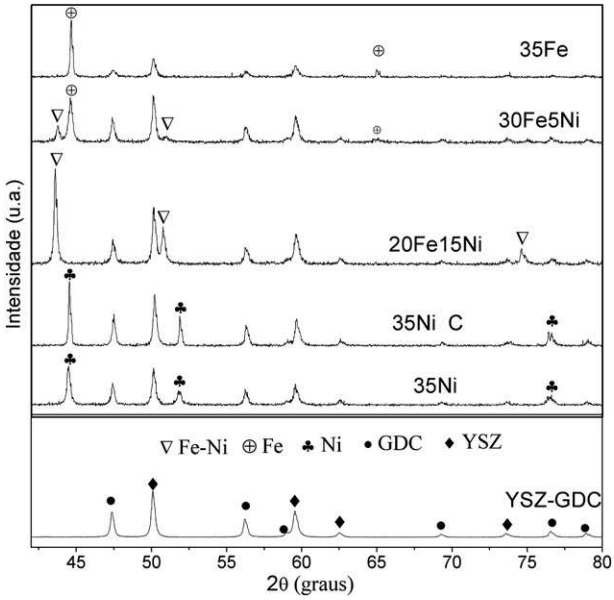

Fig. 3 – XRD patterns of composite powders after reduction (Crystallographic database of CAPES, Brazil [28]).

$2\theta = 43.60$, 50.84 and 74.69°. These data suggested the formation of a nickel-iron alloy (CAPES 26009) [28] exhibiting an FCC crystal structure. For the 30Fe5Ni sample, peaks in these same positions were also observed for this sample, indicating the formation of a nickel-iron alloy with an FCC structure. These observations suggested that the iron atoms were substituted for nickel atoms in the unit cell. Additionally, the peaks remained in the positions $2\theta = 44.72$ and 65.13°, which are characteristic of iron in the BCC crystalline form and might imply that the metallic phase of the 30Fe5Ni sample was segregated. The segregation of the phases would then form two species: a nickel-iron alloy and pure iron. In addition, the insertion of iron in the nickel crystal structure increased the unit cell volume from 43.8 Å^3 in the FCC nickel structure to 46.4 Å^3 in the FCC Ni–Fe alloy structure. Table 3 shows the crystallite sizes of nickel and iron compounds anchored on the support measured by the Scherrer equation for samples that were calcined and reduced. The data in Table 3 show that the NiO crystallites obtained with the Pechini method were significantly smaller than those obtained using the physical mixture method. For example, the Fe_2O_3 crystallite sizes were between 6.1 and 8.9 nm, showing a slight size increase with nickel loading in the sample.

A comparison of the crystallite sizes for the calcined and reduced samples showed that the crystallite size of the nickel and iron species increased after sample reduction. This size increase was probably caused by the sintering of the metallic species during the reduction process. However, it is worthwhile noting that the crystallite growth of the samples prepared using the Pechini method was lower than that observed for the samples prepared using the physical mixture method. In this synthesis method, there was little interaction between the NiO and the support, likely due to the fact that the support is a species whose isoelectric point is pH 7 and NiO is a neutral species. Therefore, there was no bond formation assistance between the NiO and the support

Table 3 – Crystallite size of iron and nickel species obtained by their XRD patterns from the Scherrer equation.

Samples	Mean crystallite size (nm)					
	Calcined samples			Reduced samples		
	NiO[a]	Fe_2O_3[b]	$NiFe_2O$[c]	Ni^{0}[d]	Fe^{0}[e]	Ni^0–Fe^0 (alloy)[d]
35Ni C	66.2	–	–	124.6	–	–
35Ni	6.2	–	–	10.2	–	–
35Fe	–	6.1	–	–	9.7	–
30Fe5Ni	No	8.2	12.4	No	16.0	16.7
20Fe15Ni	No	8.9	14.7	No	No	17.9

a Calculated using the (200) NiO plane.
b Calculated using the (104) Fe_2O_3 plane.
c Calculated using the (311) $Ni_2Fe_2O_4$ plane.
d Calculated using the (111) Ni0 and Ni 0-Fe 0 planes.
e Calculated using the (110) Fe0 plane.

for agglomeration of NiO particles, especially during the thermal treatment steps. For the Pechini method, there was also little interaction between the support and the precursor metal species as the precursor ions were trapped in a polymer network around the support in this method. This structure ensured greater dispersion and minimized crystallite growth from sintering, as suggested in Fig. 4.

Fig. 5 shows the TPR profiles for the studied materials. As can be seen, the TPR curve for the support (YSZ–GDC) showed no event associated with reduction. Previous work showed that pure YSZ also did not have any TPR activity under diluted hydrogen [49]; however, GDC samples showed evidences of reduction around 900 °C, under a diluted mixture of methane and steam [29]. In TPR analysis conditions, surface layers of a ceria monocrystal were reduced; the first monolayer showed a peak at 512 °C and the second monolayer were partially reduced at 862 °C [30].

The peaks that appeared in TPR curve of the catalyst samples were attributed to the reduction of nickel and iron species present in the composite materials. First, the different preparation methods for the monometallic nickel-based cermets led to solids with different resistances to reduction in the presence of hydrogen, evidenced by the differences in the areas delimited by the TPR peaks for the different materials. In these samples, the monometallic species that reduced in the temperature range of 410–420 °C presented weaker interactions with the support, but the converse relation might also be inferred from the data. Second, one may also observe in Fig. 5 that the reduction of both monometallic and bimetallic iron samples, displayed by multiple reduction events at temperatures above 700 °C, especially for the monometallic iron sample. In general, the reduction profile for the bimetallic samples was intermediate between those for the monometallic iron and nickel samples. Apparently the formation of the mixed oxide $NiFe_2O_4$ promoted a decrease in the maximum temperature of reduction of the bimetallic compounds, which was favored by the presence of nickel. Previous studies [31] have indicated that solids with a high concentration of oxygen vacancies usually have the ability to interact strongly with adsorbed species in their neighborhood, so the high reduction temperatures of the iron and nickel species in both the bimetallic and monometallic

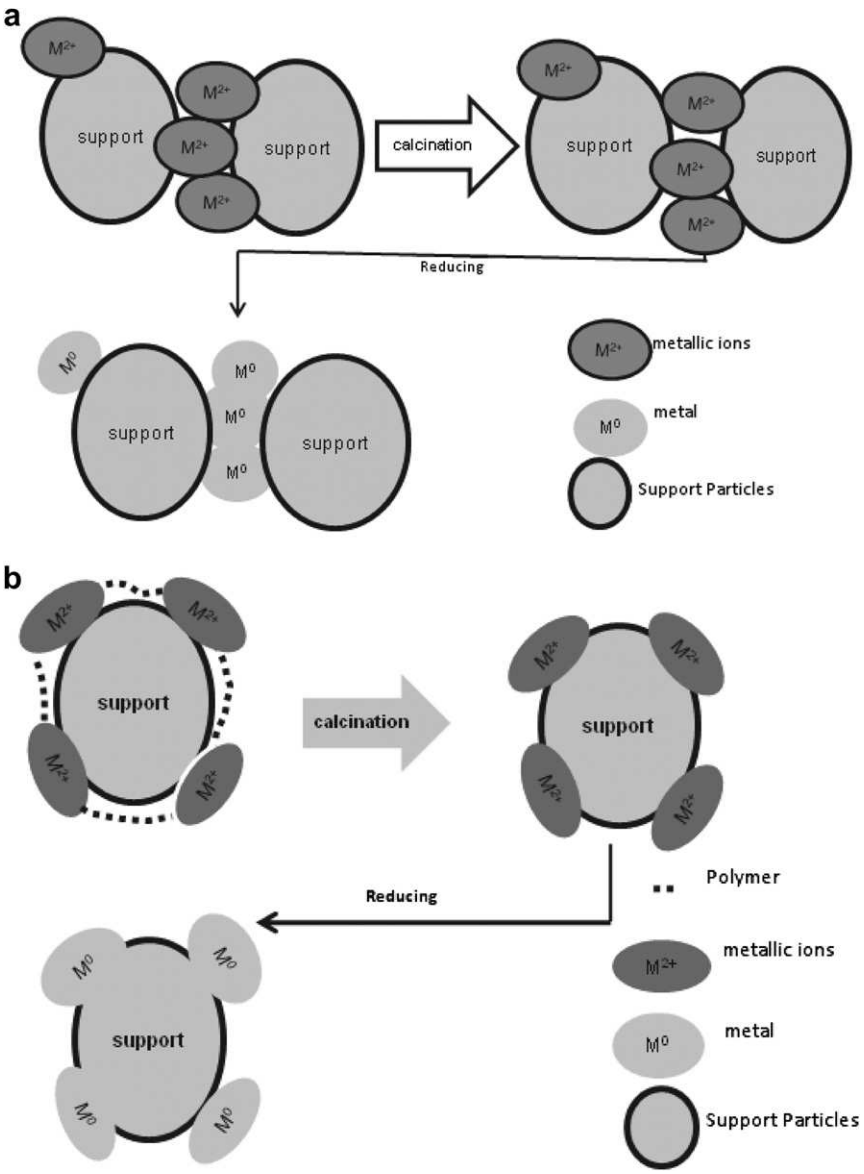

Fig. 4 – Schematic illustration of the methods of sample preparation: a) the physical mixing method; and b) the Pechini method.

iron samples were related to the strong interaction between the nickel and iron oxides with the YSZ–GDC solid. This material is believed to depict a high defect concentration [32].

For the elucidation of the peak broadening reduction, two TPR experiments under different conditions were carried out on the 35Fe sample. In the first experiment, the analysis was done at a heating rate of 10 °C min^{-1} up to 800 °C under 1.5 mol % H_2/argon and maintained at this temperature for 40 min (Fig. 6A). In the second experiment, the heating rate was held at 10 °C min^{-1} until the maximum temperature of 1100 °C was reached (Fig. 6B).

A closer inspection of Fig. 6A and B shows that the temperature is not the only important factor in the reduction of iron-supported species. The TPR curves obtained for the 35Fe sample (Fig. 6A) indicated that maintaining the sample at 800 °C for 45 min after the start of the reduction event led to the same extent of iron species reduction as those samples submitted to 1100 °C. This result may be seen by observing the areas under the TPR curves at fixed temperature (curve B) and at variable temperature (curve A). From the 80-min mark to the end of reduction, both areas were approximately equal (Fig. 6B).

As similar reduction extensions might be achieved with either fixed or variable temperature, the broadness of the iron reduction peak was probably related to hindered hydrogen diffusion in the sample, a phenomenon to which the small specific surface area of the sample (3 m^2g^{-1}) might have contributed; solids with lower porosity would require a longer hydrogen path through the bulk. The Weisz modulus [26] gives a quantitative insight about the importance of diffusion on the iron oxide reduction. At the experimental conditions of 35Fe TPR analysis, the Weisz modulus [26] was in the order of 5–10; this figure suggested that the hydrogen diffusion into the bulk iron oxide played an important role in the solid reduction. In order to calculate the Weisz modulus, the reduction rate of

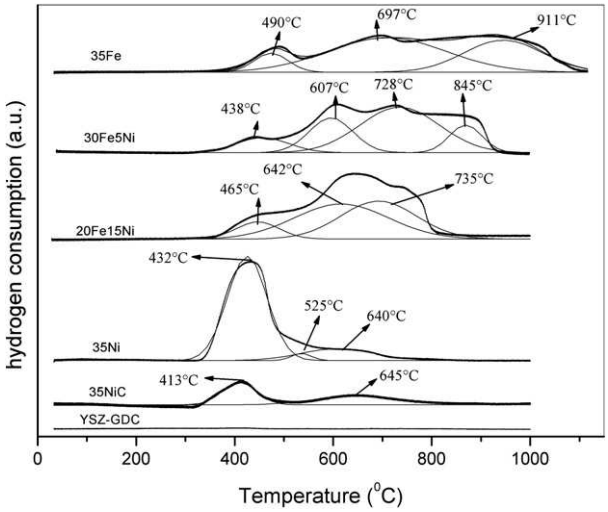

Fig. 5 – TPR profiles of the studied materials: (—) experimental profile obtained for the samples synthesized by the physical mixture or the modified Pechini methods; (…) Gaussian deconvolution of the TPR profiles.

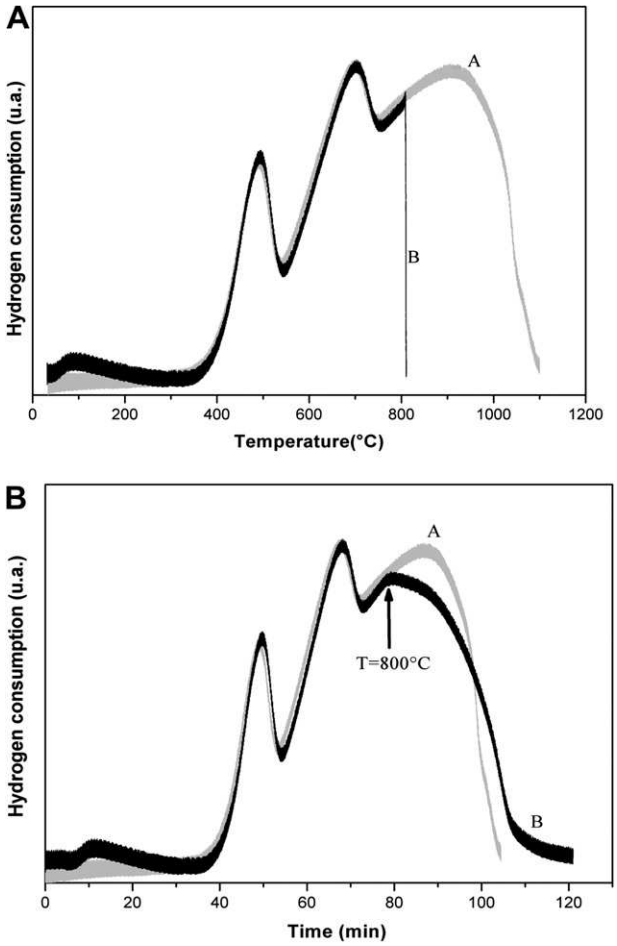

Fig. 6 – TPR profiles of monometallic iron samples calcined in air at 900 °C presented as a function of temperature (A) and time (B). For TPR curve A, the heating rate was held at 10 °C min^{-1} up to 1100 °C. For TPR curve B, the experiment was performed at the rate of 10 °C min^{-1} up to 800 °C and maintained at this temperature for 45 min.

iron oxide, about 40×10^3 $mols^{-1}$ m^{-3}, was calculated from recent data of Halim et al. [33]. The diffusion coefficient of molecular hydrogen in several materials is in the order of $1–10 \times 10^{-11}$ m^2 s^{-1} [34]. Halim et al. [33] also observed that the reduction of iron oxide particles, from the size between 30 and 150 nm, was controlled by a combined effect of chemical reaction and gaseous diffusion mechanisms.

The quantitative data obtained from the sample TPR analyses are presented in Table 4. For the monometallic nickel samples, the stoichiometric ratio of 1:1 between H_2 and Ni was considered for the quantitative evaluation of hydrogen consumption in TPR analyses according to equation (3.1).

$$NiO + H_2 \rightarrow Ni + H_2O \quad (3.1)$$

For the monometallic iron sample (35Fe), the stoichiometric relationship between molecular hydrogen and iron was 3:2 and the overall iron reduction (reaction 3.4) was the sum of reactions 3.2 and 3.3.

$$Fe_2O_3 + H_2 \rightarrow 2FeO + H_2O \quad (3.2)$$

$$2FeO + 2H_2 \rightarrow 2Fe + 2H_2O \quad (3.3)$$

$$Fe_2O_3 + 3H_2 \rightarrow 2Fe + 3H_2O \quad (3.4)$$

Finally, for the bimetallic samples, the TPR hydrogen consumption was calculated as the sum of the individual consumptions of the nickel and iron species, with each proportional to their concentration in the sample.

The data presented in Table 4 indicated that the samples prepared using the Pechini method achieved complete reduction of the metal oxides in the presence of hydrogen. In contrast, the 35NiC sample, prepared using the physical mixture method, showed a low yield in the reduction of NiO with hydrogen, reducing only 14% of the oxide initially present in the sample. This low performance might be associated with the large NiO crystallite sizes (66.2 nm) formed during the catalyst preparation, compared to the small crystallite sizes of the NiO obtained from the Pechini method. Thus, under the studied experimental conditions, only the surface of the NiO particles was converted to Ni° in the 35NiC sample. Furthermore, one may also observe from Table 4 that the metal reduction in the bimetallic samples was slightly lower than the metal reduction in the monometallic samples. This phenomenon might be explained by the fact that the individual species of NiO and Fe_2O_3 were totally reduced, whereas the $NiFe_2O_4$ species did not reach total reduction. The stronger interaction of the $NiFe_2O_4$ species with oxygen vacancies in the support might explain this observation.

This behavior might be further explained on the basis of the strong metal-support interaction (SMSI) effect between nickel and ceria, which has been amply studied. The addition of CeO_2 to a Ni/δ-Al_2O_3 catalyst increased its activity and stability for methane dry reforming; Ni catalysts with CeO_2 promoters reduced the chemical interaction between nickel and support, resulting in an increase in reducibility and high dispersion of nickel [35]. Similar study [36] has been conducted on a Ni/

Table 4 – Hydrogen mole consumption obtained from the TPR analyses, the nominal molar load of the samples and the extension of metal reduction.

Samples	TPR hydrogen total consumption of (mols × 10^{-4})	Nominal metal load (mols × 10^{-4})			Reduced metal %
		Ni	Fe	Total	
35 Ni	2.10	2.09	–	2.09	100
35 Ni C	0.30	2.09	–	2.09	14
35Fe	2.88	–	1.90	1.90	99
30Fe5NI	2.86	0.26	1.64	1.90	95
20Fe15Ni	2.64	0.72	1.01	1.72	88

δ-Al_2O_3 using a combination of cerium and zirconia as promoter; the authors ascribed this effect to the formation of NiO_x intermediates, in the promoted catalyst, which would yield high activity Ni species. Mariño et al. [37], using TPR and XPS analysis, found that the sample behavior strongly depends on the conditions of the thermal treatments. The increase in the calcination temperature of the precursors produced a strong interaction between nickel and aluminum, decreasing nickel reducibility and selectivity to C1 compounds. Ni/CeO_2 catalysts prepared by impregnation, deposition–precipitation and co-precipitation methods were used for methane decomposition [38]. The spent catalysts were analyzed by TEM, as well as temperature-programmed hydrogenation and oxidation; the Ni/CeO_2 catalyst prepared by co-precipitation method exhibited rather strong metal–support interaction probably by the formation of Ni–O–Ce solid solution, explaining its very low activity towards methane decomposition. Sánchez-Sánchez et al. [39] studied nickel catalysts supported on mixture of alumina and other metal oxide for the ethanol steam reforming. They found that TPR and XPS analyses indicated the development of strong interactions between nickel species and ZrO_2, La_2O_3 and CeO_2 oxides added to supports. La and Ce additives were found to prevent the formation of carbon filaments on nickel surfaces; these filaments were found to cause changes in product selectivities with reaction time for Zr and Mg additives, as well as bare alumina catalyst. Gonzalez-DelaCruz et al. [40] studied Ni/CeO_2 catalyst in the steam and dry reforming of methane by *in situ* XAS spectroscopy. They found that under reaction conditions at high temperature, the nickel remains completely reduced; however, under strongly reducing conditions, the nickel particles undergo unexpected changes of size and morphology. These changes were explained on the basis of strong nickel–support interaction and could also account for the higher catalyst stability observed for the dry reforming reaction. Caballero et al. [41] performed *in situ* XPS experiments with Ni nanoparticles supported on a CeO_2 thin film, using ambient pressure photoemission spectroscopy (APPES) techniques. They explained the apparent contradiction that although SMSI effects were observed but no decoration has been detected in CeO_2 supported systems by showing that hydrogen, absorbed during surface reduction of the cerium oxide, played a role in the nickel migration, through the formation of hydride-like species. As the nickel particles and the carbon impurities are both initially located at the surface of the ceria thin film used as support, the APPES results also supported the idea that it was the cerium oxide rather than the metal that migrated onto the nickel nanoparticles and carbon impurities.

3.2. *Catalyst evaluation*

The catalytic performance on the ethanol steam reforming of the developed catalysts is discussed in the following paragraphs, based on Figs. 7–10. However, some knowledge about the catalytic activity of the bare support may be helpful. Silva [49] has shown that bare YSZ displayed virtually no activity for ethanol steam reforming at temperatures around 500 °C. Godinho et al. [50] presented data for this reaction conducted over ceria nanotube and ceria powder, with a surface area of 28 and 5 $m^2\ g^{-1}$, respectively. At a reaction temperature of 500 °C, the ethanol conversion was around 75 and 55% for the

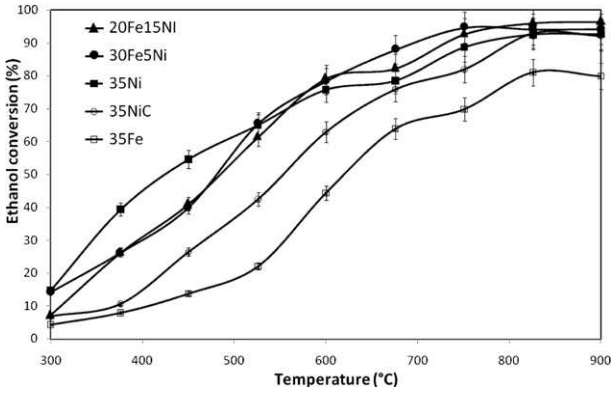

Fig. 7 – Ethanol conversion versus reactor temperature for prepared electrocatalysts. The samples were previously reduced with hydrogen and ethanol was injected at 300 °C.

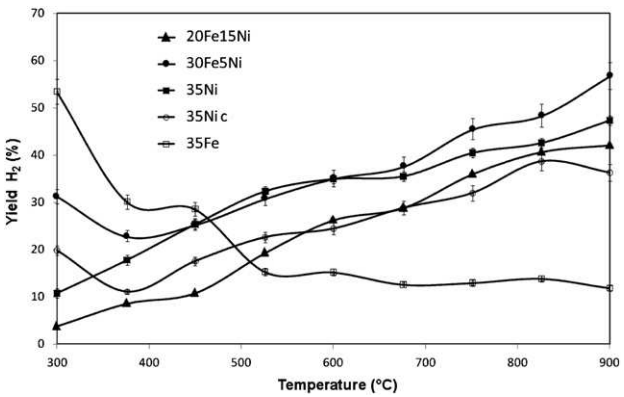

Fig. 8 – Hydrogen yield versus reactor temperature for prepared electrocatalysts.

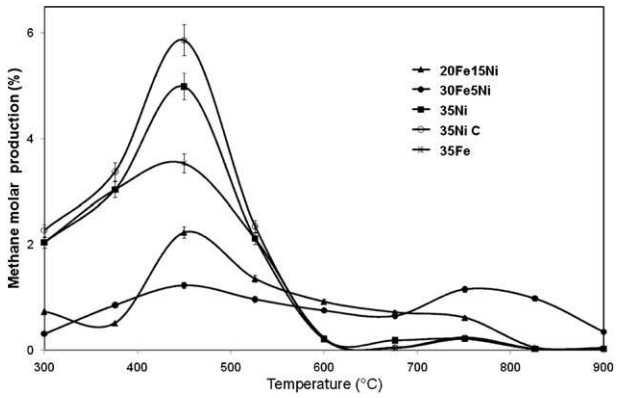

Fig. 9 – Methane production versus reactor temperature for prepared electrocatalysts.

nanotubes and powder, respectively; at 600 °C, the nanotubes presented a 100% conversion. However, ethylene was the major reaction product, varying from 30 to 50% at the reactor outlet, with much lower hydrogen production.

Fig. 7 shows the reaction temperature profiles for ethanol conversion in the steam reforming reaction catalyzed by the prepared samples. All the catalyst samples presented ethanol conversions close to or above 80% at 800 °C. Conspicuously, the 35Ni, 20Fe15Ni and 30Fe5Ni samples showed equivalent performance for ethanol conversion with no noticeable dependence on the nickel content of the sample. However, the ethanol conversion of the 35NiC sample was slightly lower than that for the 35Ni sample, indicating that there might be a lower limit to the nickel content of an active catalyst.

Fig. 8 shows the curves for hydrogen yield in the ethanol steam reforming reaction as a function of temperature. The profiles for the 35Fe sample indicated that, despite its high ethanol conversion, its hydrogen yield was very low, showing that this sample was poorly selective for hydrogen formation. Furthermore, since the hydrogen yield calculated in this work is based on the total hydrogen formed in the ethanol steam reforming (each ethanol molecule forms six hydrogen molecules), any parallel reaction will reduce the hydrogen yield.

Münster and Grabke [42] have shown that iron is almost inactive, in comparison with nickel, as catalyst for steam

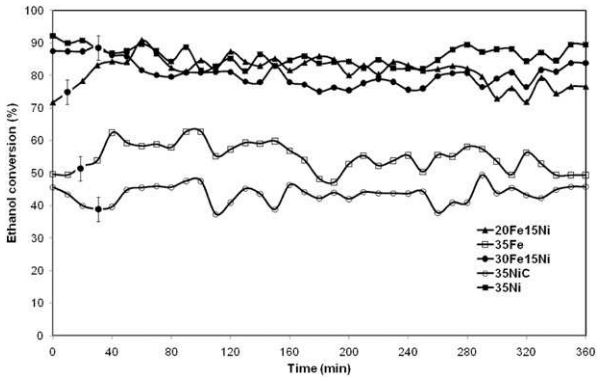

Fig. 10 – Ethanol conversion versus time on stream for prepared samples.

reforming reactions. The addition of iron to cobalt-based catalysts used in the ethanol steam reforming improved the catalyst stability but did not affect significantly the catalyst selectivity to hydrogen [43–45]. O'Shea et al. [43] found that the average hydrogen select ivies were 74.1, 74.9 and 59.4 for cobalt catalysts with no iron, 5 and 25% Fe/Co molar ratio, respectively.

Apart from the 35Fe sample, all the other samples showed similar behavior of the hydrogen yield increasing with reactor temperature. Amazingly, the 30Fe5Ni sample, with the lowest nickel load, exhibited the highest hydrogen yield at temperatures above 600 °C. This showed that pure Fe was likely not a good metal for the reforming of ethanol directly on SOFC cermet anodes.

However, this behavior might not be so surprising. Belllido et al. [31] studied the ethanol steam reforming reaction on a Ni/YSZ catalysts with 5, 10 and 15 wt.% of nickel. They observed that at 600 °C, the hydrogen concentration at the reactor outlet was 67, 66 and 72 vol.% for the catalysts with 5, 10 and 15 wt.% of Ni, respectively. At a reaction temperature of 500 °C, the hydrogen concentration was 56, 60 and 68 vol.% for the same catalysts. At 600 °C, the ethanol conversion was nearly complete for the three catalysts, while at 500 °C, the ethanol conversion was 91, 99, and 100%. Therefore, at temperatures above 500 °C, the hydrogen yield was virtually insensitive to the nickel load in the catalyst; at lower temperatures, higher Ni catalyst loads gave slightly higher hydrogen yields. Since the hydrogen production was observed to be closely independent of Ni load [31] and the carbon deposition was nearly linear with Ni load, as will be discussed in this works, one might conclude that catalysts with lower nickel load would display better performance for hydrogen yield.

Fig. 9 shows the methane production for the ethanol steam reforming, as function of reactor temperature. The methane production was measured as molar percentage of the reactor outlet stream. The methane concentration showed a maximum around 450 °C for all catalyst samples; likely due to unfavorable thermodynamics conditions for

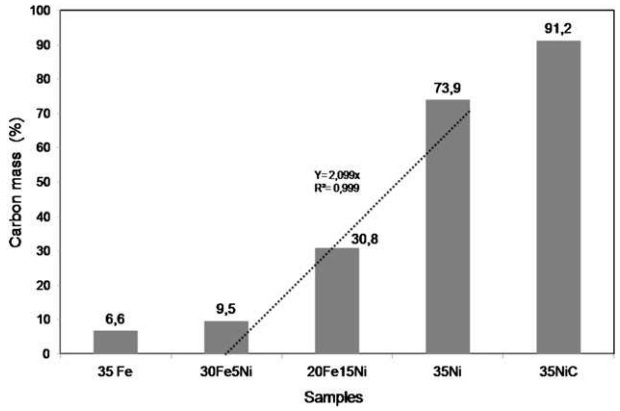

Fig. 11 – Carbon mass deposited on the electrocatalysts during the ethanol steam reforming reaction after six hours on stream at 650 °C. The mass of deposited carbon is presented as its percentage of the electrocatalyst mass. The straight line in the graph correlates carbon formation with the nickel content of the three catalysts prepared using the Pechini method.

methane conversation, which typically occurs at much higher temperatures [46]. Thereafter, methane concentration initially decreased and showed a small maximum at approximately 750 °C. Ye et al. [47] explained this behavior based on a slower methane production, during the ethanol steam reforming, and on favorable conditions for the methane steam reforming at higher temperatures.

The ethanol conversion for the steam reforming reaction at 650 °C over 6 h is shown in Fig. 10. These results indicated that the electrocatalyst remained stable during the 6-h period, with average ethanol conversion exceeding 80% for the samples containing nickel and prepared using the Pechini method. In contrast, the average ethanol conversions for the 35NiC and 35Fe samples were 43.5% and 54.8%, respectively. The average conversions reported here had standard deviations of less than 5% of their absolute values. The fluctuations observed in the ethanol conversion might mostly be due to measurement errors; the ethanol conversion increase in the initial hour on stream may be due to residual catalyst activation. Muroyama et al. [48] were found similar results. Silva [49] evaluated catalysts based on nickel and cobalt supported on YSZ in the ethanol steam reforming and found that carbon was deposited in the initial minutes on stream, remaining constant afterwards. The BET surface areas of the spent catalyst were well correlated with the amount of deposited carbon (more carbon, higher surface area). Fig. 11 presents data for carbon deposition over 6 h on the various electrocatalysts studied. The carbon mass data are presented as the percentage of the catalyst mass after reduction. These data strongly suggested that the presence of iron in the samples significantly decreased the mass of carbon deposited on the electrocatalysts. This phenomenon might be associated with the lower activity of iron compared to nickel for secondary reactions that lead to carbon formation. Furthermore, Huang et al. [3], studying a composite of nickel and iron supported on ScSZ exposed to ethanol vapor for 24 h, found that carbon deposits increased as the nickel loading increased.

The preparation method of the electrocatalyst also influenced its activity to catalyze reactions that led to carbon formation. The 35NiC sample prepared using the physical mixture method formed 17% more carbon than the 35Ni sample prepared using the Pechini method. This result might be related to the size of metal crystallites (i.e., larger crystallites displayed a greater tendency for carbon formation), suggesting that the carbon formation reaction might be classified as a "demanding" reaction (following Boudart's classification of demanding and facile reactions) [23]. As a final important point, the samples containing nickel and prepared using the Pechini method exhibit a surprisingly linear correlation between the mass of deposited carbon and the nickel content in the sample.

The rapid deposition of carbon at nickel cermets is probably the major hindrance for SOFC directaly fed with ethanol [2]. A further inspection of the literature on the subject will bring valuable insight. Carbon deposition on different catalyst was found to be very sensitive to the reaction temperature, although contradictory results have been reported. Vizcaíno et al. [51] found that the carbon was approximately 30 wt.% up to 500 °C and 50 wt.% above 550 °C, with a slight increase with temperature; they studied the ethanol steam reforming reaction over Cu–Ni supported on silica. Similar result was found by Denis et al. [52] studying the same reaction catalyzed with nickel supported on different metal oxides. These authors found that the catalyst with 27 wt.% of iron did not show any improvement toward carbon deposition; however they used other method for the catalyst preparation. On the other hand, Chen and Liu [53] found a carbon deposition of 22 and 7 wt.% for the ethanol steam reforming carried out for 10 h at 550 and 650 °C, respectively; they used a perovskite-type catalyst of nickel, iron and lanthanum. Sekine et al. [44] found that iron addition to $Co/SrTiO_3$ catalyst reduced six-fold the carbon formation in the ethanol steam reforming.

The size of nickel crystallites was also found to play an important role in carbon formation; generally smaller crystallites produced less carbon. Sánchez-Sánchez et al. [39] used nickel supported on alumina mixed with different metal oxides to study the ethanol steam reforming; they explained the higher coke production on the catalyst containing zirconia based on the larger size of its nickel crystallites. Nonetheless, these authors used a very different approach to explain the lower carbon formation on the catalysts containing either ceria or lanthana. Ceria may increase the available surface oxygen to enhance the surface oxidation reactions of carbon precursors; the interaction between nickel and lanthanum species may prevent coke deposition by reaction with lanthanum oxycarbonate. Vizcaíno et al. [51] found that the addition of copper to nickel catalysts prevented carbon formation; they explained this effect suggesting that copper atoms preferentially eliminated large ensembles of Ni metal atoms necessary for carbon deposition. Li et al. [38] studied the carbon formation from methane over Ni/CeO_2 catalysts prepared by different methods; the catalyst activity was correlated with the size of the nickel crystallites, which varied from 20 to 30 nm.

The characteristics of the catalyst support were found to be very important in the catalyst activity for carbon deposition. Vizcaíno et al. [54] found that the Mg addition to Ni/alumina catalyst reduced the carbon formation in the ethanol steam

Table 5 – Catalyst evaluation on ethanol steam reforming reaction [average values, $T = 650$ °C, time-on-stream = 6 h, molar water/ethanol = 3].

Samples	Ethanol conversion %	Hydrogen yield %	Carbon formation, (carbon/catalyst) wt.%
35Ni	44	15	91
35Ni C	86	40	74
35Fe	81	34	31
20Fe15Ni	81	35	9
30Fe5Ni	55	3	6

Table 6 – Catalyst evaluation on ethanol steam reforming reaction, literature data.

Catalyst	Reference	Temperature, °C	Water/ethanol, molar	Ethanol conversion %	Hydrogen yield %	Carbon formation, (carbon/catalyst) wt.%
10%Ni/Zn + Na	[52]	650	4	20	55 (1)	10
17%Ni/La–Fe	[53]	650	3	100	73	74
15%NiO/MgO	[53]	650	3	–	–	190
$NiFe_2O_4$	[48]	550	6	100	48	Observed
5%Ni/($CeO_2Al_2O_3$)	[55]	600	3	98	47	10
50%Ni/YSZ	[10]	500	3	100	65	Observed
Cu_2–Ni_{14}/SiO_2	[51]	600	3.7	100	40	44
Cu_2–Ni_{14}/Al_2O_3	[51]	600	3.7	99	16	60
Cu_2–Ni_{14}/MCM-41	[51]	600	3.7	100	53	27
35%Ni/Al_2O_3	[54]	650	5.5	100	83	52
35%(Ni + Mg)/Al_2O_3 [Ni/Mg = 10]	[54]	650	5.5	99	83	54
35%(Ni + Mg)/Al_2O_3 [Ni/Mg = 2]	[54]	650	5.5	98	80	28

reforming by half; this effect was attributed to the neutralization of acid sites of the support, avoiding ethanol dehydration. Sodium addition to Ni/alumina catalyst almost completely suppressed carbon deposition in the ethanol steam reforming, since sodium strongly inhibited the ethanol dehydration [52]. However, the catalyst activity for steam reforming was correlated with the carbon formation; generally it was found that low catalytic performance for ethanol reforming was related with low activity in coke formation [51,52].

TEM studies of spent catalyst after carbon deposition from methane [38] showed that some nickel particles were on the top of the carbon nanofibers, explaining the low catalyst deactivation with carbon deposition. The catalyst stability might also depend on the gasification ability of the carbonaceous species [40].

3.3. *Catalyst data comparison*

Table 5 gives the ethanol steam reforming performance on at 650 °C of the catalysts prepared in this work. The figures were the average over a period of 6 h on stream, as the data presented in Fig. 10. Table 6 gives the catalyst performance for the same reaction presented in the literature; the original reported data were adjusted for comparison.

Although some care is needed in comparing data from different sources, the comparison can be very illustrative. For all reported catalysts, excluding one, the ethanol conversion was around 100% in the reaction temperature ranging from 500 to 650 °C; the catalysts developed in this work presented maximum ethanol conversion around 80–90%. The hydrogen yield showed a much higher variation among the studied catalysts and might chiefly reflect the water to ethanol ratio; if one selects the catalysts evaluated at a water/ethanol molar ratio equal to three, only the catalysts developed by Chen and Liu [53] and Resini et al. [10] presented hydrogen yield higher than that displayed by the catalysts in this work. However, the former had a metal load much lower than that required by a SOFC anode (around 35 wt.%); the later presented an usually high nickel load (50 wt.%), with no qualitative data about carbon formation.

Finally, the catalysts presented in Table 6 might be classified by their carbon formation activity. The first class would encompass the catalysts forming above 40 wt.% of carbon; they are inadequate as SOFC anode. The second class, the two catalysts developed by Vizcaíno et al. [51,54]; however, one catalyst had a low metal load and the other was tested with high water/ethanol ratio. The third class, the catalysts developed by Denis et al. [52] and Profeti et al. [55] with little carbon formation activity; however, both catalysts had a low metal load too low for SOFC anode. The catalysts 20Fe15Ni and 30Fe5Ni of this were in second and third classes, both adequate for SOFC anode on carbon formation basis.

4. Conclusions

The Pechini method studied here for the synthesis of Ni–Fe/YSZ–GDC composites was successfully used to produce powders with crystallographic and morphological characteristics suitable for use in SOFC anodes. On the other hand, materials prepared using the physical method displayed limitations in particle size, reducibility and hydrogen production. The samples prepared by Pechini method present nickel crystallites with diameter in the range of 10–20 nm after reduction. The small nickel crystallites are more easily reducible than the larger ones.

The nickel and iron deposited on the support form an alloy after reduction under diluted hydrogen; this alloy is slightly lesser reducible than the individual metals. However, it interacts strongly with the support, improving its catalytic performance for the ethanol steam reforming and reducing its activity for carbon formation.

The catalysts developed in this work present good hydrogen yield on the ethanol steam reforming, comparable to catalysts reported in the literature. The catalyst performance is nearly independent of its nickel load, down to figures as low as 5 wt.%. However, the carbon formed on the catalysts is linearly correlated with their nickel load. The catalyst with low nickel load, but total metal contents as high as 35 wt.%, produced very little carbon, comparable to some of the best catalysts reported in the literature but with much lower metal load.

Therefore, the Ni–Fe/YSZ–GDC composites developed in this work are highly promising cermets for application as SOFC anodes, as they have a very high hydrogen yield in the ethanol steam reforming and very low carbon formation, along with high metal load.

Acknowledgements

The authors gratefully acknowledge grants from the Brazilian Ministry of Science and Technology (MCT) to support this work. They are especially grateful to Rede PaCOS (Grant 01.06.0901.00) and Rede Norte/Nordeste de Catálise (RECAT, Grant 22.02.0289.00), supported by FINEP/CT-PETRO. The authors also acknowledge FAPESB (MAS) and CNPq (RPF) for helpful scholarships.

REFERENCES

[1] Hecht ES, Gupta GK, Zhu H, Dean AM, Kee RJ, Maier L, et al. Methane reforming kinetics within a Ni–YSZ SOFC anode support. Applied Catalysis A: General 2005;295: 40–51.
[2] Atkinson A, Barnett S, Gorte RJ, Irvine JTS, McEvoy AJ, Mogensen M, et al. Advanced anodes for high-temperature fuel cells. Nature Materials 2004;3:17–27.
[3] Huang B, Wang SR, Liu RZ, Wen TL. Preparation and performance characterization of the Fe-Ni/ScSZ cermet anode for oxidation of ethanol fuel in SOFCs. Journal of Power Sources 2007;167:288–94.
[4] Douvartzides SL, Coutelieris FA, Demin AK, Tsiakaras PE. Electricity from ethanol fed SOFCs: the expectations for sustainable development and technological benefits. International Journal of Hydrogen Energy 2004;29:375–9.
[5] Macedo IC, Seabra JEA, Silva JEAR. Green house gases emissions in the production and use of ethanol from sugarcane in Brazil: the 2005/2006 averages and a prediction for 2020. Biomass & Bioenergy 2008;32:582–95.
[6] Park SD, Vohs JM, Gorte RJ. Direct oxidation of hydrocarbons in a solid-oxide fuel cell. Nature 2000;404:265–7.
[7] Venancio SA, Gutierres TF, Sarruf BJM, Miranda PEV. Direct oxidation of ethanol in SOFC anodes. Materia-Rio De Janeiro 2008;13:560–8.
[8] Ye XF, Wang SR, Hu Q, Chen JY, Wen TL, Wen ZY. Improvement of Cu–CeO_2 anodes for SOFCs running on ethanol fuels. Solid State Ionics 2009;180:276–81.
[9] Cimenti M, Hill JM. Direct utilization of ethanol on ceria-based anodes for solid oxide fuel cells. Asia-Pacific Journal of Chemical Engineering 2009;4:45–54.
[10] Resini C, a Delgado MCH, Presto S, Alemany LJ, Riani P, Marazza R. Yttria-stabilized zirconia (YSZ) supported Ni–Co alloys (precursor of SOFC anodes) as catalysts for the steam reforming of ethanol. International Journal of Hydrogen Energy 2008;33:3728–35.
[11] Jiang SP, Chan SH. A review of anode materials development in solid oxide fuel cells. Journal of Materials Science 2004;39: 4405–39.
[12] Amado RS, Malta LFB, Garrido FMS, Medeiros ME. Solid oxide fuel cells: materials, components and configurations. Quimica Nova 2007;30:189–97.
[13] Zhao XY, Yao Q, Li SQ, Cai NS. Studies on the carbon reactions in the anode of deposited carbon fuel cells. Journal of Power Sources 2008;185:104–11.
[14] Mermelstein J, Millan M, Brandon NP. The impact of carbon formation on Ni–YSZ anodes from biomass gasification model tars operating in dry conditions. Chemical Engineering Science 2009;64:492–500.
[15] Gavrielatos I, Drakopoulos V, Neophytides SG. Carbon tolerant Ni–Au SOFC electrodes operating under internal steam reforming conditions. Journal of Catalysis 2008;259: 75–84.
[16] La Rosa D, Sin A, Lo Faro M, Monforte G, Antonucci V, Arico AS. Mitigation of carbon deposits formation in intermediate temperature solid oxide fuel cells fed with dry methane by anode doping with barium. Journal of Power Sources 2009;193:160–4.
[17] Baker RTK. Catalytic growth of carbon filaments. Carbon 1989;27:315–23.
[18] Koh J-H, Yoo Y-S, Park J-W, Lim HC. Carbon deposition and cell performance of Ni–YSZ anode support SOFC with methane fuel. Solid State Ionics 2002;149:157–66.
[19] Park HC, Virkar AV. Bimetallic (Ni–Fe) anode-supported solid oxide fuel cells with gadolinia-doped ceria electrolyte. Journal of Power Sources 2009;186:133–7.
[20] Martins RF, Brant MC, Domingues RZ, Paniago RM, Sapag K, Matencio T. Synthesis and characterization of NiO–YSZ for SOFCs. Materials Research Bulletin 2009;44:451–6.
[21] Ribeiro NFP, Souza M, Neto ORM, Vasconcelos SMR, Schmal M. Investigating the microstructure and catalytic properties of Ni/YSZ cermets as anodes for SOFC applications. Applied Catalysis A-General 2009;353:305–9.
[22] Duncan H, Abu-Lebdeh Y, Davidson IJ. Study of the cathode-electrolyte interface of $LiMn_{1.5}Ni_{0.5}O_4$ synthesized by a sol–gel method for Li-ion batteries. Journal of the Electrochemical Society 2010;157:A528–35.
[23] Silva MA, Alencar MGF, Fiuza RP, Boaventura JS. Preparação e Avaliação de Célula a Combustível do Tipo PaCOS Unitária com Ânodo a base de Níquel e Cobalto. Revista Matéria 2007; 12:72–85.
[24] Burton AW, Ong K, Rea T, Chan IY. On the estimation of average crystallite size of zeolites from the Scherrer equation: A critical evaluation of its application to zeolites with one-dimensional pore systems. Microporous and Mesoporous Materials 2009;117:75–90.
[25] Ligiero CBP, dos Reis LA, Parrilha GL, Baptista M, Canela MC. Comparison of quantification methods in gas chromatography: an experiment for chemistry courses. Quimica Nova 2009;32:1338–41.
[26] Hill CG. Introduction to chemical engineering kinetics and reactor design. New York: Wiley; 1977.
[27] Figueredo JL, Ribeiro FR. Catálise heterogênea. 2nd ed. Lisbone: Fundação Calouste Gulbenkain; 2007.
[28] Coordenação de Aperfeiçoamento de Pessoal de Nível Superior (CAPES, Brazilian Agency for the Advancement of High Eduction) (2009) http://www.capes.gov.br, accessed on December 03, 2009.
[29] RamIrez-Cabrera E, Atkinson A, Chadwick D. Catalytic Steam Reforming of Methane Over $Ce_{0.9}Gd_{0.1}O_{2-x}$. Applied Catalysis B: Environmental 2004;47:127–31.
[30] Holgado JP, Alvarez R, Munuera G. Study of CeO_2 XPS spectra by factor analysis: reduction of CeO_2. Applied Surface Science 2000;161:301–15.
[31] Bellido JDA, Assaf EM. Nickel catalysts supported on ZrO_2, Y_2O_3-stabilized ZrO_2 and CaO-stabilized ZrO_2 for the steam reforming of ethanol: effect of the support and nickel load. Journal of Power Sources 2008;177:24–32.
[32] Goodenough JB. Oxide-ion electrolytes. Annual Review of Materials Research 2003;33:91–128.
[33] Halim KSA, Khedr MH, Soliman NK. Reduction characteristics of iron oxide in nanoscale. Materials Science and Technology 2010;26:445–52.

[34] Pyun SI, Park JW, Yoon YG. Hydrogen permeation through PECVD (plasma-enhanced chemical vapor deposition) TiO_2 film on Pd by the time lag method. Journal of Alloys and Compounds 1995;231:315–20.
[35] Wang SB, Lu GQ. Role of CeO_2 in $Ni/CeO_2–Al_2O_3$ catalysts for carbon dioxide reforming of methane. Applied Catalysis B-Environmental 1998;19:267–77.
[36] Roh HS, Jun KW, Park SE. Methane-reforming reactions over $Ni/Ce–ZrO_2$/theta–Al_2O_3 catalysts. Applied Catalysis A-General 2003;251:275–83.
[37] Marino F, Baronetti G, Jobbagy M, Laborde M. Cu-Ni–K/gamma–Al_2O_3 supported catalysts for ethanol steam reforming Formation of hydrotalcite-type compounds as a result of metal-support interaction. Applied Catalysis A-General 2003;238:41–54.
[38] Li Y, Zhang BC, Tang XL, Xu YD, Shen WJ. Hydrogen production from methane decomposition over Ni/CeO_2 catalysts. Catalysis Communications 2006;7:380–6.
[39] Sánchez-Sánchez MC, Navarro RM, Fierro JLG. Ethanol steam reforming over $Ni/M_xO_y–Al_2O_3$ (M = Ce, La, Zr and Mg) catalysts: influence of support on the hydrogen production. International Journal of Hydrogen Energy 2007;32:1462–71.
[40] Gonzalez-DelaCruz VM, Holgado JP, Pereniguez R, Caballero A. Morphology changes induced by strong metal-support interaction on a Ni-ceria catalytic system. Journal of Catalysis 2008;257:307–14.
[41] Caballero A, Holgado JP, Gonzalez-delaCruz VM, Habas SE, Herranz T, Salmeron M. In situ spectroscopic detection of SMSI effect in a Ni/CeO_2 system: hydrogen-induced burial and dig out of metallic nickel. Chemical Communications 2010;46:1097–9.
[42] Munster P, Grabke HJ. Kinetics of the steam reforming of methane with iron, nickel, and iron-nickel alloys as catalysts. Journal of Catalysis 1981;72:279–87.
[43] O'Shea VAD, Nafria R, de la Piscina PR, Homs N. Development of robust Co-based catalysts for the selective H-2-production by ethanol steam-reforming. The Fe-promoter effect. International Journal of Hydrogen Energy 2008;33:3601–6.
[44] Sekine Y, Kazama A, Izutsu Y, Matsukata M, Kikuchi E. Steam reforming of ethanol over cobalt catalyst modified with small amount of iron. Catalysis Letters 2009;132:329–34.
[45] Torres JA, Llorca J, Casanovas A, Dominguez M, Salvado J, Montane D. Steam reforming of ethanol at moderate temperature: multifactorial design analysis of Ni/La_2O_3-Al_2O_3, and Fe- and Mn-promoted Co/ZnO catalysts. Journal of Power Sources 2007;169:158–66.
[46] Abbas HF, Daud W. Hydrogen production by methane decomposition: a review. International Journal of Hydrogen Energy 2010;35:1160–90.
[47] Ye XF, Wang SR, Wang ZR, Xiong L, Sun XE, Wen TL. Use of a catalyst layer for anode-supported SOFCs running on ethanol fuel. Journal of Power Sources 2008;177:419–25.
[48] Muroyama H, Nakase R, Matsui T, Eguchi K. Ethanol steam reforming over Ni-based spinel oxide. International Journal of Hydrogen Energy 2010;35:1575–81.
[49] Silva MA. Célula a combustível do tipo SOFC a etanol com reforma direta. Master's thesis, Universidade Federal da Bahia, Instituto de Química, Salvador – Bahia, 2007.
[50] Godinho M, Gonçalves RF, Leite ER, Raubach CW, Carreño HLV, Probst LFD, et al. Gadolinium-doped cerium oxide nanorods: novel active catalysts for ethanol reforming. Journal of Materials Science 2010;45:593–8.
[51] Vizcaíno AJ, Carrero A, Calles JA. Hydrogen Production by Ethanol Steam Reforming Over Cu–Ni Supported Catalysts. International Journal of Hydrogen Energy 2007; 32:1450–61.
[52] Denis A, Grzegorczyk W, Gac W, Machocki A. Steam reforming of ethanol over Ni/support catalysts for generation of hydrogen for fuel cell applications. Catalysis Today 2008; 137:453–9.
[53] Chen SQ, Liu Y. $LaFe_yNi_{1-y}O_3$ supported nickel catalysts used for steam reforming of ethanol. International Journal of Hydrogen Energy 2009;34:4735–46.
[54] Vizcaíno AJ, Arena PB, Baronetti G, Carreroa A, Callesa JA, Laborde MA, et al. Ethanol steam reforming on Ni/ Al_2O_3 catalysts: effect of mg. International Journal of Hydrogen Energy 2008;33:3489–92.
[55] Profeti LPR, Ticianelli EA, Assaf EM. Production of hydrogen via steam reforming of biofuels on $Ni/CeO_2–Al_2O_3$ catalysts promoted by noble metals. International Journal of Hydrogen Energy 2009;34:5049–60.